Proceedings of the NROCK 2023
The IV Nordic Symposium on
Rock Mechanics and Rock Engineering
ISBN 978-9935-9436-2-0
DOI 10.33112/nrock2023.11

Size Dependancy of Post-peak Stress-Strain Properties of Rocks

Abbas Taheri (abbas.taheri@queensu.ca)

A. Taheri
Queen's University, Kingston, Canada

J. Zhang
Formerly The University of Adelaide, Australia

ABSTRACT

Post-peak behavior of rock is significant to the stability of surface and underground rock excavations and the performance of drilling and excavation operations. Mechanical properties and damage characteristics of rocks are subjected to the measurement scale. The effect of size on sandstone's post-peak behavior and failure characteristics are investigated during monotonic uniaxial compressive loading. A series of tests were undertaken on sandstone samples with an aspect ratio of 2.5 and diameters of 19mm, 30mm, 42mm, and 63mm. The lateral strain-controlled loading method was adopted to capture the post-peak stress-strain characteristics. The three-dimensional digital image correlation (3D DIC) technique is utilized to investigate field strain patterns and local damage. The brittleness index was found to increase with an increase in diameter, indicating that the rock sample was damaged in a more brittle regime with a larger size. 3D DIC results demonstrated that in the pre-peak regime, the specimen deforms uniformly. In the pos-peak regime, however, the specimen shows localized behavior. This behavior is different for samples having different diameters. The overall post-peak was a combination of class I and class II behavior.

KEYWORDS
Sandstone; Post-peak; Brittleness; Digital Image Correlation, Damage

INTRODUCTION

Scale effect, which is defined by the influence of the absolute size (i.e., diameter) of cylinder samples when the aspect ratio is constant, may have considerable influence on rock properties. The effects of scale on rock strength have been investigated by several researchers (Bahaaddini et al. 2014; Darlington et al. 2011; Pan et al. 2009; Yoshinaka et al. 2008; Zhang et al. 2011). However, contradictory results are observed. Some scholars reported that scale effects do exist, and an increase in diameter leads to a reduction in rock strength (Cunha 1990; Jackson and Lau 1990). Other researchers observed no scale effects on rock strength (Thuro et al. 2001; Pells 2004). Masoumi et al. (2015) observed that the uniaxial compressive strength of Gosford sandstone first increased and then decreased in the diameter range of 19mm to 145mm. The studies mentioned above mainly focused on the strength of different rocks under scale effects. However, there are limited studies on the impact of scale on the post-peak stress-strain relations and the localized behavior of rocks after the peak stress point.

The complete stress-strain relation of rocks (i.e., the pre-peak and the post-peak behaviors) is considered a prominent tool in rock mechanics to describe strain energy evolution and for rock brittleness determination (Shirani Faradonbeh et al. 2021). The post-peak stress-strain curve of rock is detrimental to the stability of surface and underground rock excavations. For instance, rock post-failure behavior defines the energy released after failure, contributing to rock bursts in deep excavations. In addition, the rock complete stress-strain curve is significant in investigating the performance of drilling and excavation operations (Munoz et al. 2016c). Therefore, characterizing the post-peak behavior of rocks associated with localized behavior is critical to many rock Engineering applications (Munoz et al. 2016a).

Deformation localization is the intrinsic cause of rock failure and strain burst. Therefore, micro-cracking due to the applied load that leads to increased localized damage needs to be investigated thoroughly. This is mainly because the existing micro-cracks inside the rock create homogenous damage zone distributions in the rock mass. It would be interesting to investigate the effect of the scale of localized behavior of rock in the post-peak regime. To accurately investigate rock stress-strain behavior after the peak stress and localization behavior, in this study, a non-contact strain measurement method, i.e., three-dimensional digital image correlation (3D DIC), is utilized to investigate the post-peak stress-strain behavior and local damage of rock specimens with different diameters. This method makes 3D displacements and strains available at every point on the specimen's surface. The DIC method has been implemented to study the deformation of rock materials (Tung et al. 2013; Cheng et al. 2017; Munoz and Taheri 2017; Zhang et al. 2018; Zhou et al. 2019).

A series of uniaxial compression tests were carried out on sandstone specimens having different diameters, with an aspect ratio of 2.5. The lateral strain-controlled method was used to obtain the post-peak stress-strain behavior. Effects of scale on post-peak stress-strain characteristics were investigated. Strain energy development and brittleness index evolution under scale effects were presented. Finally, the 3D DIC method is utilized to study the field of axial and lateral strains during compression.

1. MATERIAL AND METHODS

1.1. Specimen preparation

Hawkesbury sandstone, a medium-strong sedimentary rock, is used as the testing material. Hawkesbury sandstone is an early Middle Triassic (Anisian) formation widely exposed in the Sydney Basin in Australia. The rock has an average uniaxial compressive strength (UCS) of 44 MPa and an average density of 2260 kg/m^3. All the rock samples were drilled from the same rock block and in a similar direction. Rock specimens with an aspect ratio (i.e., a length to diameter) of 2.5 and diameters of 19 mm, 30 mm, 42 mm, and 63 mm, are prepared. The diameter is more than 20 times larger than the grain size, satisfying the ISRM testing method recommendation (Fairhurst and Hudson 1999). The end surfaces and sides of rock specimens were prepared smooth and straight, as recommended by the ISRM.

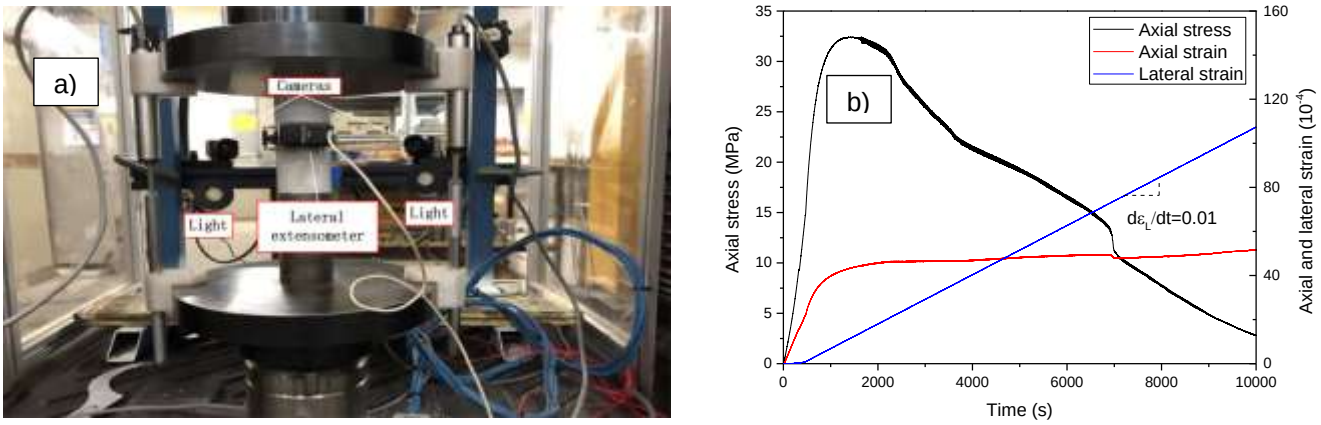

Figure 1. Experimental methodology; a) Test set-up; b) Time history of axial stress, axial and lateral strains in the lateral strain-controlled tests.

1.2. Uniaxial compression tests

Before the load tests, the rock specimens were instrumented by a lateral strain extensometer placed along the perimeter. To eliminate the end-edge friction effects, the lateral extensometer was mounted at the middle length of the specimens (see Figure 1a). During the compression test, the axial deformation of specimens was recorded by a pair of axial linear variable displacement transducers (LVDTs) attached on both the left and right sides of the specimen. A lighting system is used to shed additional light on the sample surface to capture the deformation of the sample using DIC cameras.

The rock specimens were loaded monotonically by a closed-loop servo-controlled hydraulic compressive machine (Type: Instron 1342 manufactured by Instron Inc.). The maximum loading capacity of the testing machine is 250kN. The lateral strain-controlled method loaded the rock specimens using the lateral strain extensometer. Figure 1b shows a typical test's time history of axial stress, axial strain, and lateral strain. As demonstrated in this figure, a constant lateral strain rate of 0.01×10^{-4}/s was used in the lateral strain-controlled tests.

1.3. Digital Image Correlation measurement

A detailed introduction of 3D Digital Image Correlation (DIC) application to uniaxial compression tests can be found in the first author's previous studies (i.e. Munoz et al. 2016a, b). Therefore, here, only a brief description is provided.

3D DIC is a non-contact optical method that measures surface deformation. A pair of high-resolution digital cameras (Type: Fujinon HF75SA-1, 1:1.8/75mm, 5 Megapixels resolution) was used to capture the images of the speckled surface of the sample. The speckle pattern on the rock samples should be created before the test. The sample surface was first sprayed with ordinary white paint and then spray-tarnished black paint. Then, each camera was calibrated using a 30mm standard target with uniformly spaced markers (see Figure 2a). During the loading test, the cameras captured images at a frame rate of an image per second during loading. The captured images were then processed by VIC-3D software to acquire the deformations and strain values (Sutton et al. 2009). To investigate the field strain patterns and local damage of rock samples, five virtual extensometers (i.e., DIC-E0, DIC-E1, DIC-E2, DIC-E3, and DIC-E4) were selected as presented in Figure 2b.

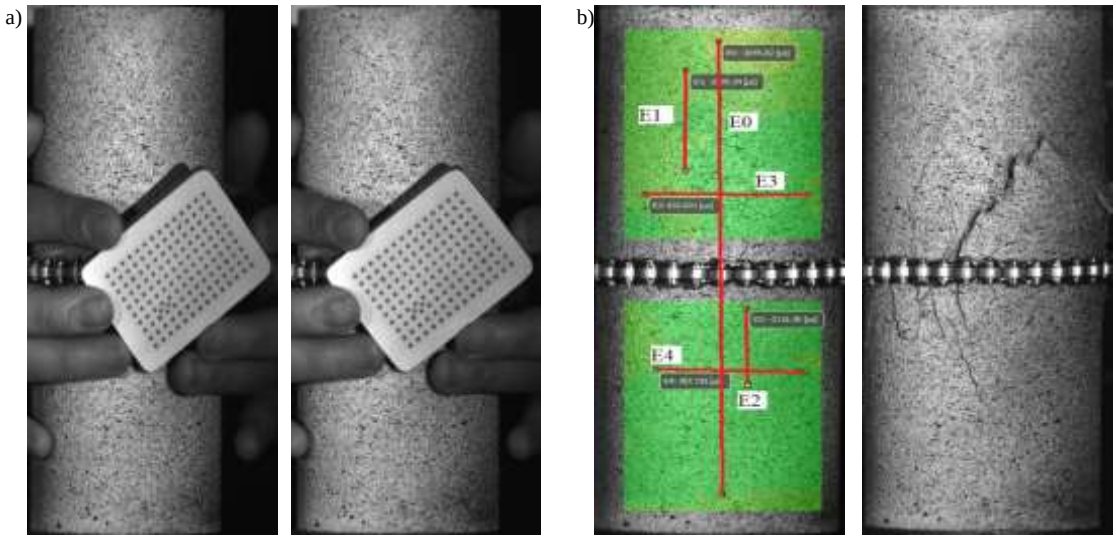

Figure 2. DIC measurement: a) Calibration procedure of the cameras' left and right pair imaging and b) location of virtual extensometers within the area of interest and rock failure during the test.

2. POST-PEAK STRESS-STRAIN CHARACTERISTICS

The stress-strain curves are normalized to investigate the dependency of scale effects on the post-peak behavior under uniaxial loading conditions, as shown in Figure 3. The normalized stress-strain curves were obtained by dividing the stresses and strains by peak stress and peak strain at failure.

The curves demonstrated in Figure 3, in general, show that in the post-peak regime, the stress-strain characteristics for samples with a diameter of 63mm showed a combination of class I and class II behavior based on the classification proposed by Wawersik and Fairhurst (1970). And the post-peak stress-strain curves almost overlapped with each other. The same phenomenon is also found in the samples with diameters of 42mm and 30mm. However, for the samples with a 19mm diameter, two showed a predominant class I behavior, and one had a dominant class II behavior.

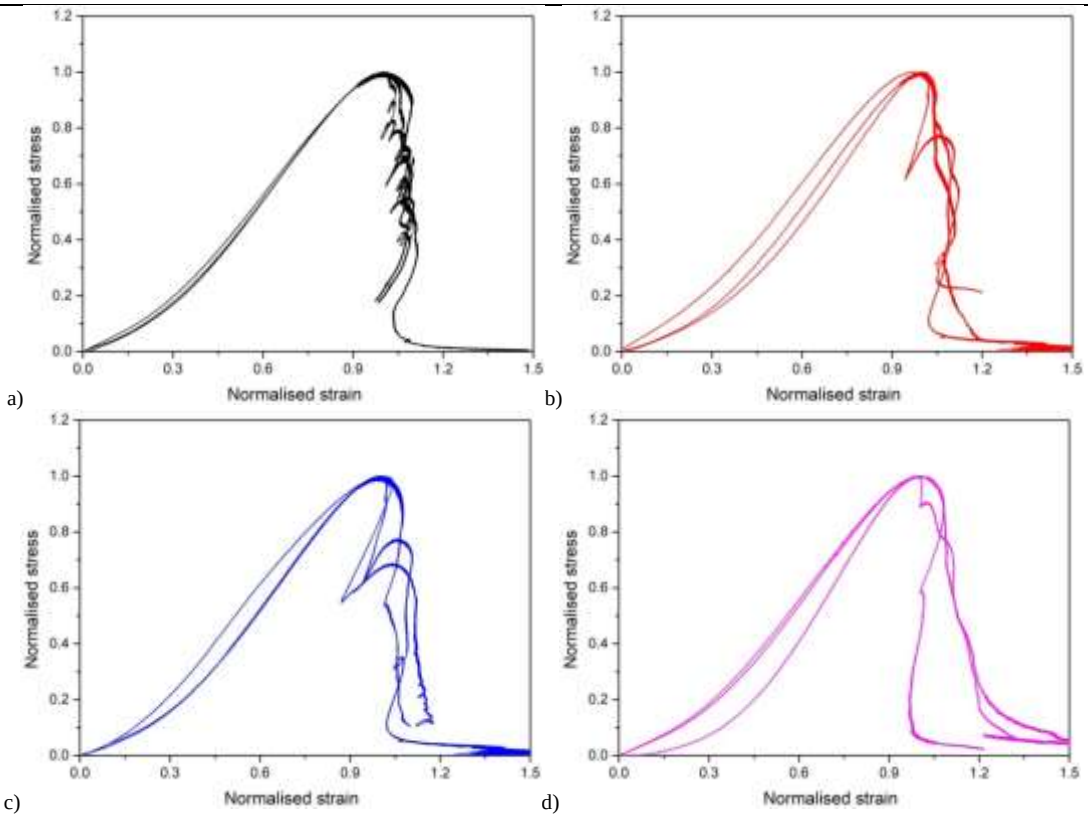

Figure 3, Normalized stress-strain relation of sandstone with different diameters: a) 63mm, b) 42mm, c) 30mm, and d) 19mm.

3. STRAIN ENERGY-BASED BRITTLENESS INDEX

Strain energy, or the amount of energy absorbed by a unit volume of rock under compression, is an important parameter to assess the rock's brittle behavior (Munoz et al. 2016b). The energy absorption capability is also essential when the rock is subjected to blast loads and impacts (Bažant et al. 2004). Variations of different strain energies in the experimental results are investigated to investigate the effect of sample size on the pre-peak and post-peak stress-strain behavior. Figure 4 and Equations 3a-c, demonstrate how pre-peak strain energy U_{pre}, peak strain energy U_{peak}, post-peak strain energy $U_{post,}$ and elastic strain energy U_e are derived. U_{pre} was estimated by the area under the stress-strain curve enclosed by loading the specimen up to the peak stress and then unloading it entirely. E is Young's modulus obtained by LVDTs. U_{post} as shown in Fig. 5a, is post-peak strain energy. A post-peak stress level of $1/3\sigma_f$ is recommended by Munoz et al. (2016a) to calculate U_{post}. U_e, which can be expressed by Equation 3a, is the strain energy consumed in the specimen when the failure point is reached (see Figure 4b). On the other hand, the peak strain energy U_{peak} and the total strain energy U_{total} can be expressed by Equations 3b and 3c as follow:

$$U_e = \frac{\sigma_f^2}{2E_{LVDT}} \quad (3a)$$

$$U_{peak} = U_{pre} + U_e \quad (3b)$$

$$U_{total} = U_{pre} + U_{post} \quad (3c)$$

Rock brittleness is an essential parameter to characterize the brittle fracture of rocks. Many brittleness indices were proposed by different scholars (Altindag 2008; Hajiabdolmajid and Kaiser 2003; Munoz et al. 2016b). In this study, three fracture energy-based brittleness indices proposed by the the first author (Munoz et al. 2016a) were adopted to describe the brittle fracture behavior under the scale effects. The brittleness indices were defined as follows:

$$B_1 = \frac{U_e}{U_{total}} \quad (3d)$$

$$B_2 = \frac{U_e}{U_{post}} \quad (3e)$$

$$B_3 = \frac{U_{peak}}{U_{total}} \quad (3f)$$

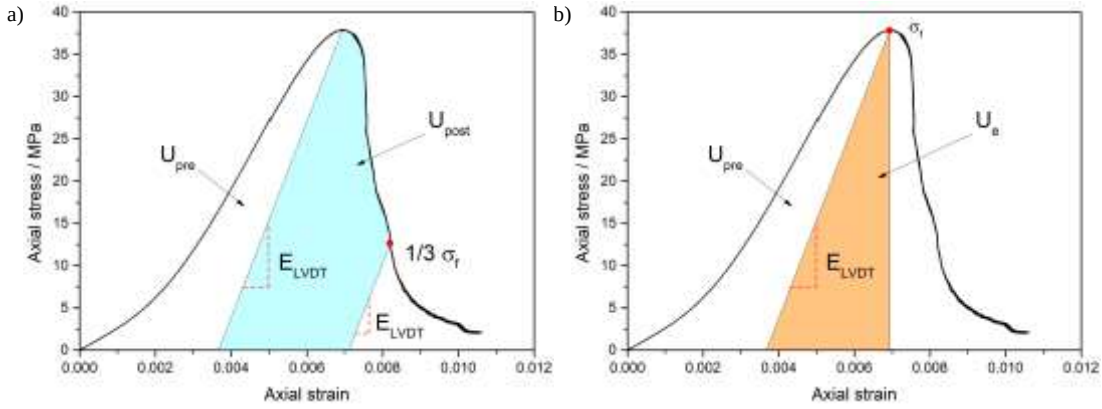

Figure 4, Strain energy of rock specimen under uniaxial compression: a) U_{pre} and U_{post}, and b) U_e

The three brittleness indices were calculated using the strain energy values and plotted in Figure 5. A higher brittleness index means the rock is more brittle. It can be seen from the figure that the three brittleness indices increased almost linearly with an increase in the sample diameter. This indicated that when the size of the rock sample is large, the rock exhibits more brittle behavior when subjected to uniaxial loading.

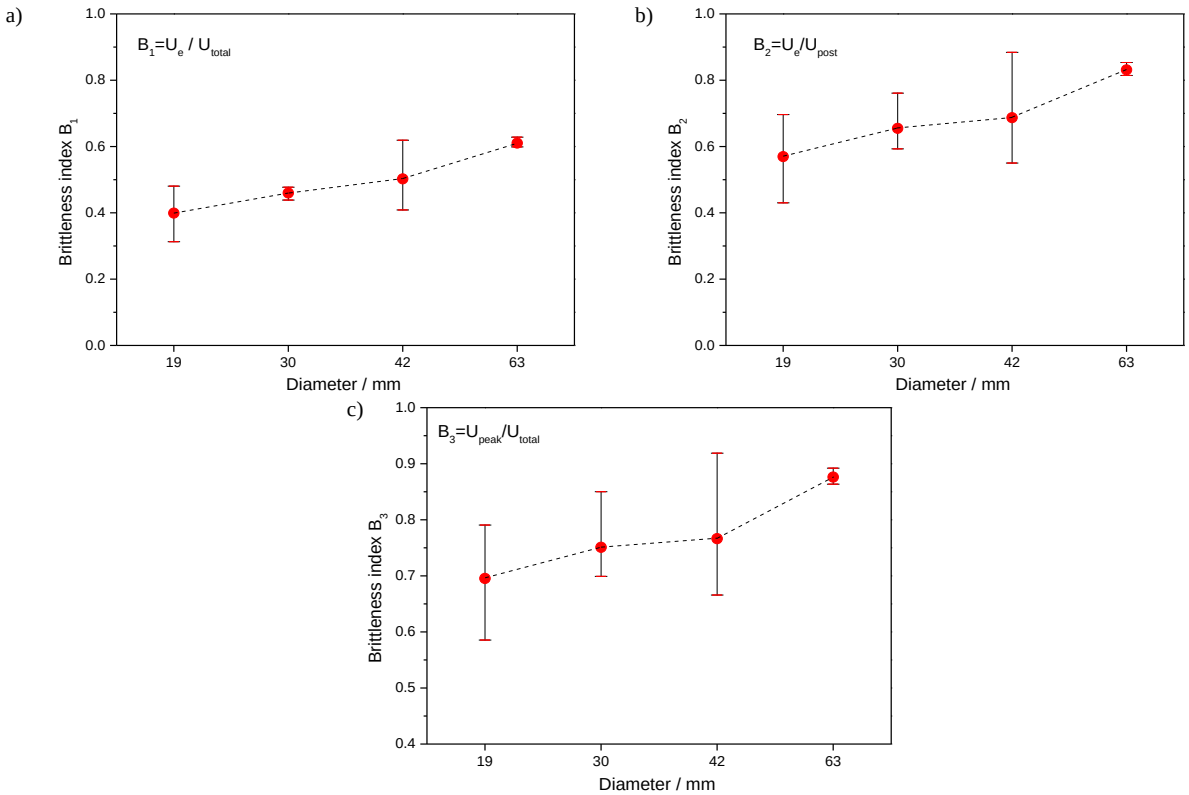

Figure 5, Scale effect on brittleness indices: a) B_1, b) B_2, and c) B_3

4. LOCALIZATION DURING UNIAXIAL LOADING

Eight stress levels (i.e., four in the pre-peak regime and four in the post-peak regime) were selected to show the field strain patterns of rock samples with different diameters. The four stress levels in the pre-peak regime are crack closure stress σ_{cc}, crack initiation stress σ_{ci}, crack damage stress σ_{cd} and peak stress σ_f which were identified from the volumetric strain-axial stress and crack volumetric strain-axial strain curves (Taheri et al. 2020). The four stress levels in the post-peak regime were $0.9\sigma_f$, $0.75\sigma_f$, $0.6\sigma_f$, and $0.4\sigma_f$.

Figure 6a shows the field of axial strain development of samples with a diameter of 42mm. The stress-strain curves obtained from LVDTs and virtual extensometers are compared. The virtual extensometers E0, E1, and E2, located vertically along the rock sample, are applied to measure the axial field strains. Due to the inherent bedding error in the axial strain results measured by the LVDT the virtual strain gauges show lower strain values in the pre-peak regime. In contrast, E3 and E4, located horizontally, are used to measure lateral field strains. The lateral strain values measured by these virtual extensometers are consistent in pre-peak and are slightly higher than the strain measured by the chain extensometer. The results obtained by the virtual extensometers indicate that in the pre-peak regime, the rock deformed uniformly. By comparing the color gradient of axial strain in the samples at different pre-peak stress levels in Figure 6b, i.e., most of the area of interest was found in two color patterns, it demonstrated the axial strain developed uniformly in pre-peak stage, which is consistent with the stress-strain curves measured by virtual extensometers.

As can be seen in Figure 6a, in the post-peak regime the virtual extensometers, the axial LVDT and the lateral chain extensometer follow the same trend until the strength is almost 23 MPa. After that the post-peak stress-strain curves of virtual extensometers, LVDT and chain extensometer are remarkably different. This is due to the development of the localization of strains (either axial, lateral) within the specimen. This results are consistent with the observation of field of axial strains demonstrated in Figure 6c. The results show that E2 and E4 are mainly located inside the localized damage zone and therefore the stress-strain behavior is class I strain softening. Whereas the other virtual extensometers are mostly outside of the localized damage zone and therefore demonstrate unloading and mostly a class II behavior. Axial LVDT and the chain extensometers demonstrate the overall post-peak behavior of the specimen. The overall failure behavior which is demonstrated by the external LVDT is a combination of class I and class II behavior.

Figures 7a-c presents the field of axial strains in the post-peak regime for specimens with diameters of 63mm, 30mm, and 19mm at the selected stress levels introduced before. As can be seen in these figures and Figure 6c, localization of strains around the shear bands have occurred at $\sigma=0.75\sigma_f$ for 63mm and 42mm samples and at $\sigma=0.6\sigma_f$ for 30mm specimen. 19mm specimen shows localization in the post-peak regime, however, no clear shear band is observable. This might be due to the small DIC measurement area when the sample size is considerably small. This demonstrates that the post-peak strain fields are significantly affected by the absolute size of the specimen.

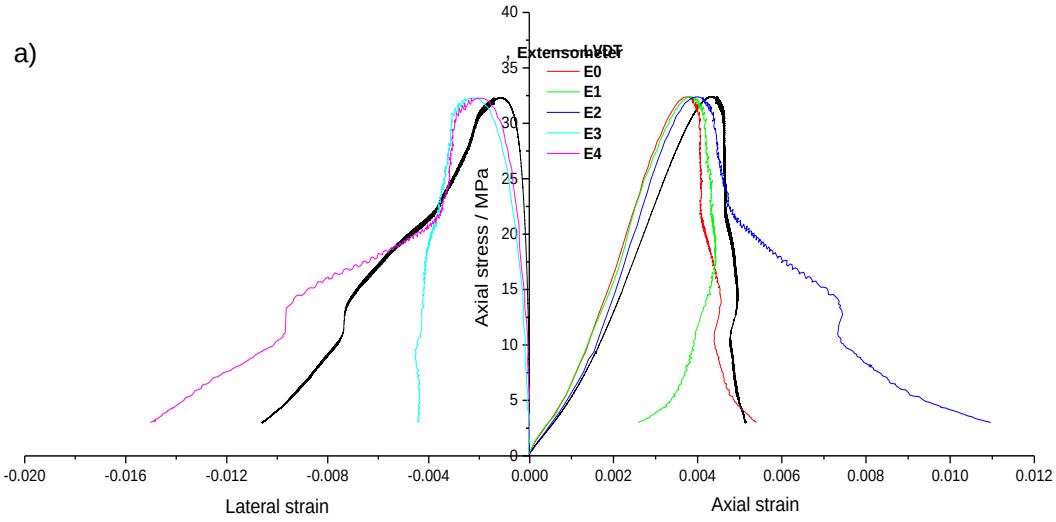

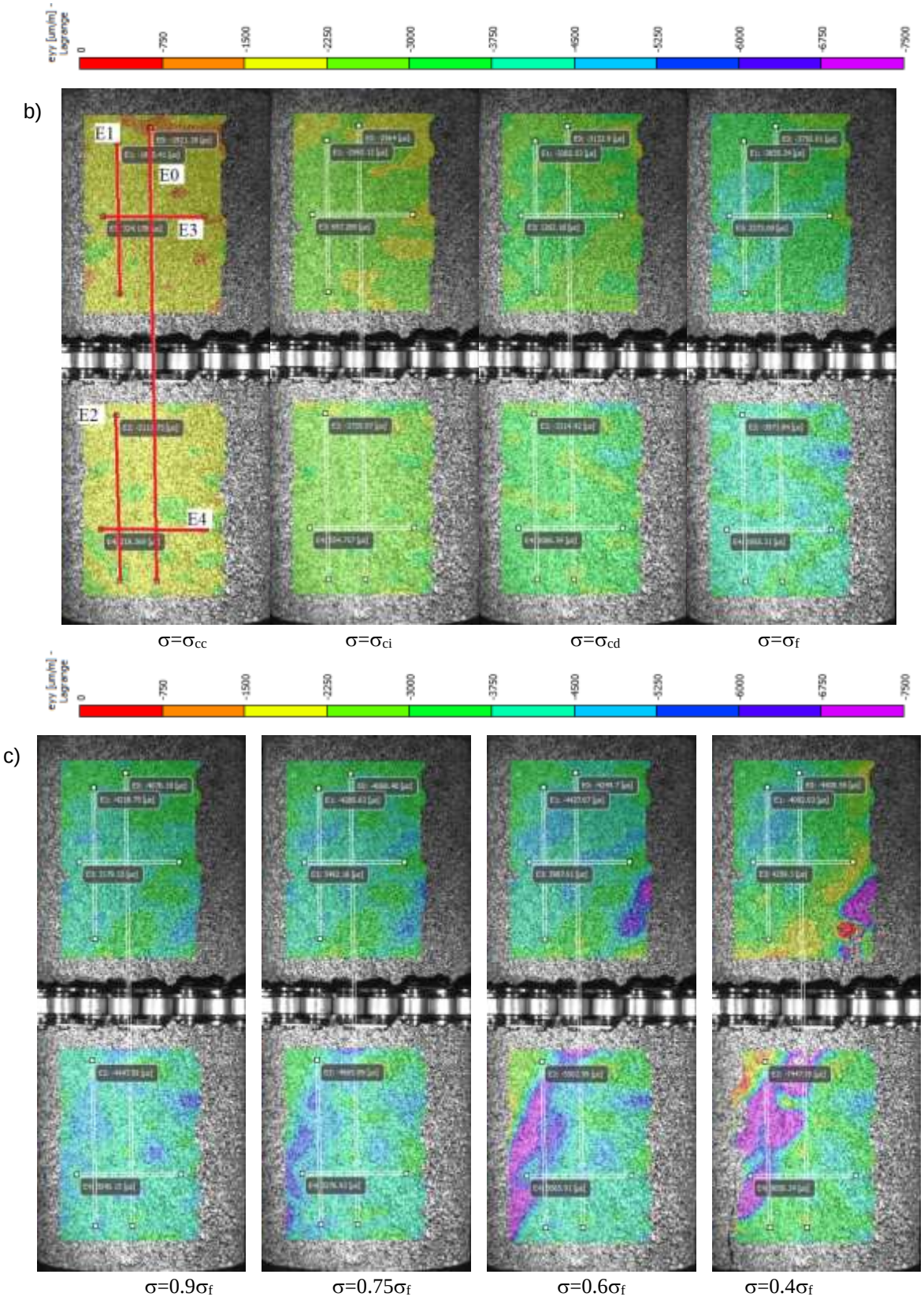

Figure 6, Stress-strain results of 42mm specimen: a) Stress-strain relation by axial LVDT, lateral extensometer, and virtual extensometers; b) Field of axial strains development in the pre-peak regime, and c) Field of axial strains development in the post-peak regime.

a)

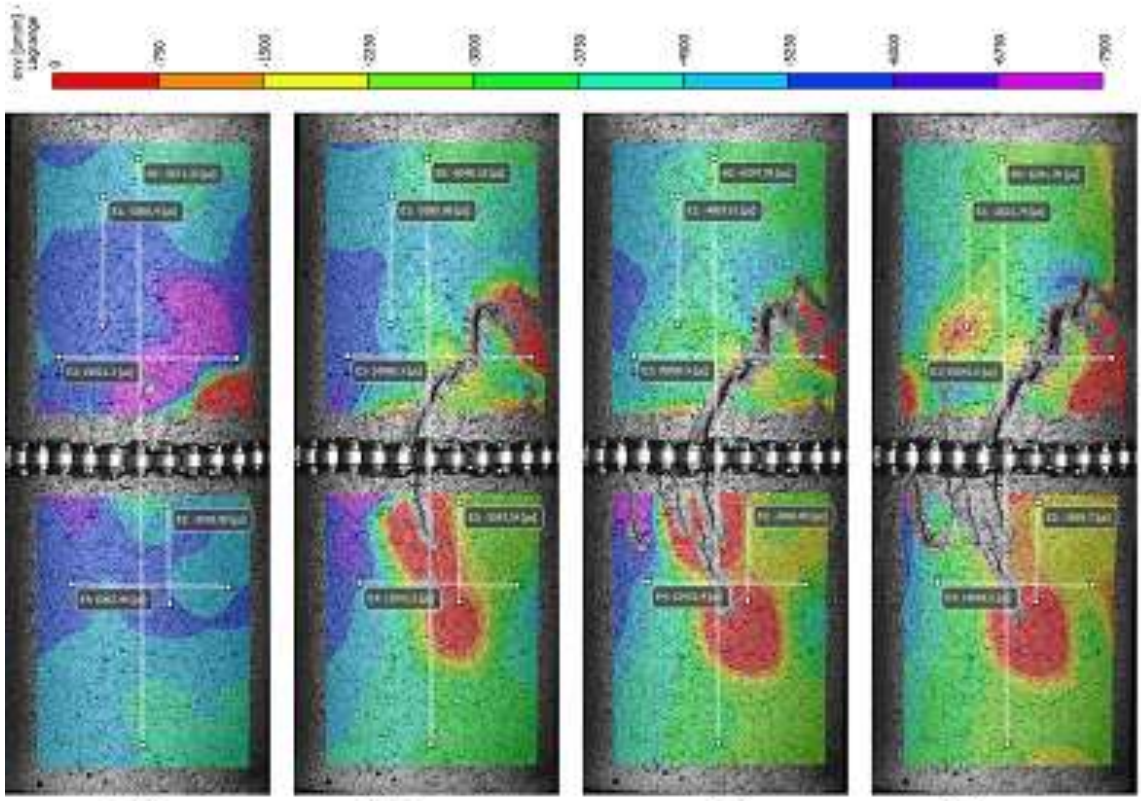

b)

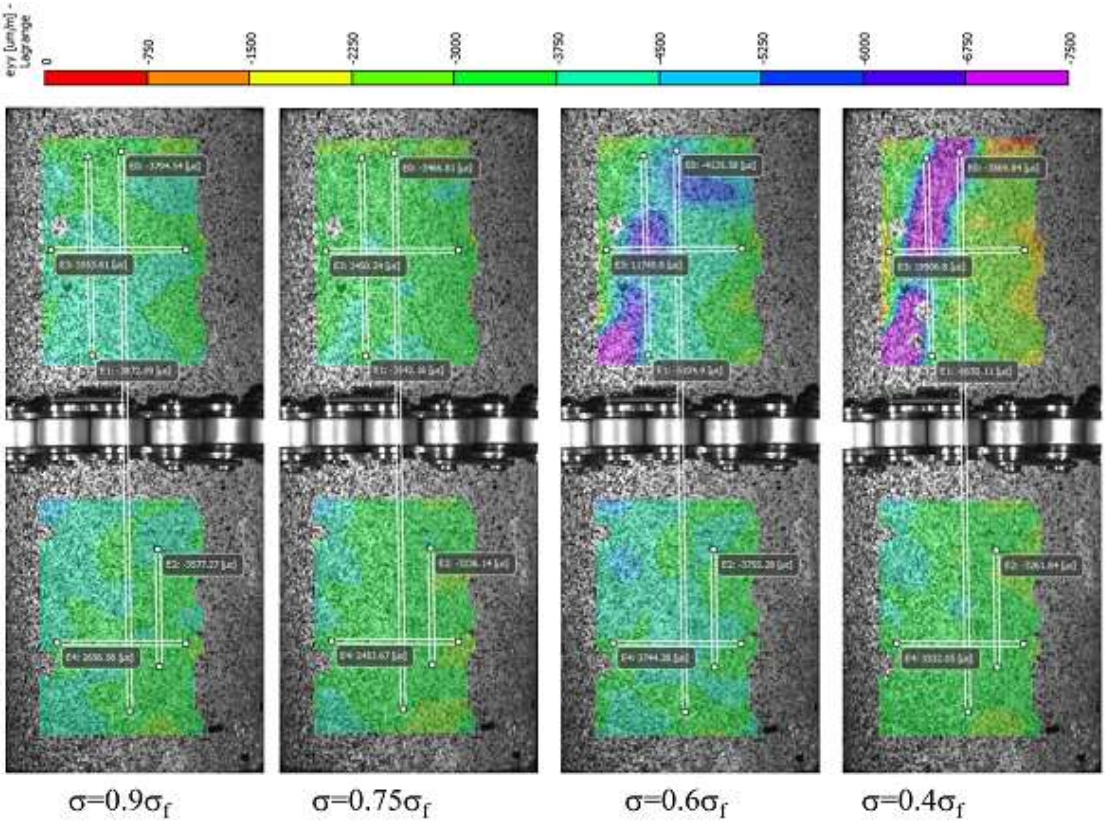

c)

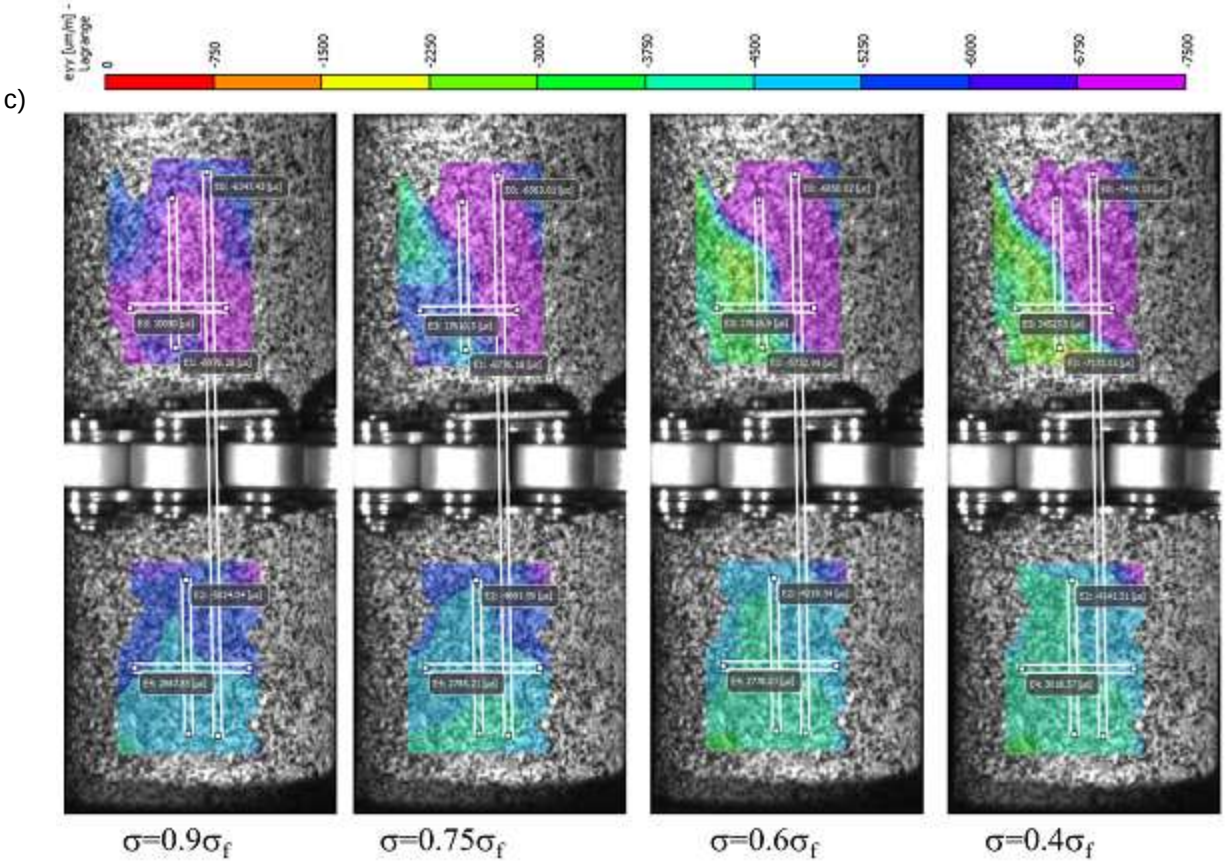

Figure 7. Field of axial strain developed in the post-peak regime for specimens: a) 63mm, b)30mm, and c)19mm.

5. CONCLUSIONS

Size effects on the mechanical properties, post-peak stress-strain behaviors, and field strain patterns were investigated under uniaxial compression. The lateral controlled method is adopted to capture the complete post-peak stress-strain relation of Hawkesbury sandstone. In addition, the three-dimensional digital image correlation (3D DIC) technique is used to examine the strain patterns and fracture characteristics. A series of tests were conducted on sandstone samples with a constant aspect ratio of 2.5 and different diameters. The following conclusions were drawn from this study:

1. The failure behavior of samples having different sizes is mainly a combination of class I and class II behavior.
2. By increasing the diameter of the rock sample, strain energy-based brittleness indices demonstrated that the rock exhibits more brittle behavior under uniaxial compression loading.
3. Rock in axial and lateral directions shows uniform deformation in the pre-peak regime, and strain localization occurs in the post-peak regime.
4. In general, the trend of the field of axial strain in the sample with different diameters was different. In the post-peak regime, localization around the shear bands occurs at 75% of peak strength for 63mm and 42mm samples and at 60% of peak strength for the 30mm specimen.19mm specimen did not show a clear shear band in 3D DIC measurements.

REFERENCES

Altindag, R. (2008). *Relationships between brittleness and specific energy in excavation mechanics*. International proceedings of 9th regional rock mechanics symposium, Izmir, Turkey, 437-451.

Bahaaddini, M., Hagan, P., Mitra, R. & Hebblewhite, B. (2014). Scale effect on the shear behaviour of rock joints

based on a numerical study. *Engineering Geology*, 181, 212-223.
Bažant, Z.P., Barr, B., de Borst, R., Burtscher, S.L., Buyukozturk, O., Carol, I., Carpinteri, A., et al. (2004). Quasibrittle fracture scaling and size effect. *Materials and Structures*, 37, 547-568
Cheng, J.-L., Yang, S.-Q., Chen, K., Ma, D., Li, F.-Y. & Wang, L.-M. (2017). Uniaxial experimental study of the acoustic emission and deformation behavior of composite rock based on 3D digital image correlation (DIC). *Acta Mechanica Sinica*, 33, 999-1021.
Cunha, A.P. (1990). *Scale Effects in Rock Masses*: Proceedings of the First International Workshop on Scale Effects in Rock Masses, Loen, Norway, 7-8 June 1990. AA Balkema.
Darlington, W.J., Ranjith, P.G. & Choi, S. (2011). The effect of specimen size on strength and other properties in laboratory testing of rock and rock-like cementitious brittle materials. *Rock Mechanics and Rock Engineering*, 44, 513-529.
Fairhurst, C. & Hudson, J. (1999). Draft ISRM suggested method for the complete stress-strain curve for intact rock in uniaxial compression. *International Journal of Rock Mechanics and Mining Sciences*, 36, 279-289.
Hajiabdolmajid, V. & Kaiser, P. (2003). Brittleness of rock and stability assessment in hard rock tunneling. *Tunnelling and Underground Space Technology*, 18, 35-48.
Jackson, R. & Lau, J. (1990). *The effect of specimen size on the laboratory mechanical properties of the Lac du bonnet grey granite*. Procceeding of the first international workshop on scale effects in rock masses. Balkema (AA), 165-174.
Masoumi, H., Saydam, S. & Hagan, P.C. (2015). Unified size-effect law for intact rock. *International Journal of Geomechanics*, 16, 04015059.
Munoz, H. & Taheri, A. (2017). Specimen aspect ratio and progressive field strain development of sandstone under uniaxial compression by three-dimensional digital image correlation. *Journal of Rock Mechanics and Geotechnical Engineering*, 9, 599-610.
Munoz, H., Taheri, A. & Chanda, E. (2016a). Pre-peak and post-peak rock strain characteristics during uniaxial compression by 3D digital image correlation. *Rock Mechanics and Rock Engineering*, 49, 2541-2554.
Munoz, H., Taheri, A. & Chanda, E. (2016b). Fracture energy-based brittleness index evelopment and brittleness quantification by pre-peak strength parameters in rock uniaxial compression. *Rock Mechanics and Rock Engineering*, 49, 4587-4606.
Munoz, H., Taheri, A., Chanda, E. (2016c) Rock drilling performance evaluation by an energy dissipation based rock brittleness index. *Rock Mechanics and Rock Engineering*, 49: 3343–3355.
Pan, P.-Z., Feng, X.-T. & Hudson, J.A. (2009). Study of failure and scale effects in rocks under uniaxial compression using 3D cellular automata. *International Journal of Rock Mechanics and Mining Sciences*, 46, 674-685.
Pells, P. (2004). On the absence of size effects for substance strength of Hawkesbury Sandstone. *Australian Geomechanics*, 39, 79-83.
Shirani Faradonbeh, R. Taheri, A, Karakus M. (2021) Failure behaviour of a sandstone subjected to the systematic cyclic loading: Insights from the double-criteria damage-controlled test method. Rock Mechanics and Rock Engineering, 54, 5555–5575.
Sutton, M.A., Orteu, J.J. & Schreier, H. (2009). *Image correlation for shape, motion and deformation measurements: basic concepts, theory and applications*. Springer Science & Business Media.
Taheri, A., Zhang, Y., Munoz, H. (2020). Performance of rock crack stress thresholds determination criteria and investigating strength and confining pressure effects, *Construction and Building Materials*, 243, 118263.
Thuro, K., Plinninger, R., Zäh, S. & Schütz, S. (2001). *Scale effects in rock strength properties. Part 1: Unconfined compressive test and Brazilian test*. EUROCK 2001: Rock Mechanics-A Challenge for Society, 169-174.
Tung, S.-H., Weng, M.-C. & Shih, M.-H. (2013). Measuring the in situ deformation of retaining walls by the digital image correlation method. *Engineering Geology*, 166, 116-126,
Wawersik, W. & Fairhurst, C. (1970). A study of brittle rock fracture in laboratory compression experiments. *International Journal of Rock Mechanics and Mining Sciences & Geomechanics Abstracts*. 7, 561-564.
Yoshinaka, R., Osada, M., Park, H., Sasaki, T. & Sasaki, K. (2008). Practical determination of mechanical design parameters of intact rock considering scale effect. *Engineering Geology*, 96, 173-186.
Zhang, G., Xing, Y. & Wang, L. (2018). Comprehensive sandstone fracturing characterisation: Integration of fiber Bragg grating, digital imaging correlation and acoustic emission measurements. *Engineering Geology*, 246, 45-56,
Zhang, Q., Zhu, H., Zhang, L. & Ding, X. (2011). Study of scale effect on intact rock strength using particle flow modeling. *International Journal of Rock Mechanics and Mining Sciences*, 48, 1320-1328.
Zhou, X.-P., Wang, Y.-T., Zhang, J.-Z. & Liu, F.-N. (2019). Fracturing Behavior Study of Three-Flawed Specimens by Uniaxial Compression and 3D Digital Image Correlation: Sensitivity to Brittleness. *Rock Mechanics and Rock Engineering*, 52, 691-718.